MICROSTRUCTURE STUDIES OF NIOBIUM*

D. Baars#, T. Bieler, MSU Dept. Chem. Eng. & Mat. Sci., East Lansing, MI, U.S.A.
P. Darbandi, F. Pourboghrat, MSU Dept. Mech. Eng., East Lansing, MI, U.S.A.
C. Compton, NSCL, East Lansing, MI, U.S.A.

Abstract

Superconducting radio frequency (SRF) cavities are often formed from fine-grain niobium sheet which is heavily deformed and heat treated throughout processing Identification of relationships between the deformed, recovered, and recrystallized microstructure are required to guide production of niobium in a metallurgical state that is optimal for cavity performance. To gain understanding of deformation mechanisms in high purity niobium that will support development of constitutive models, and to establish relationships between defect structures and recrystallization processes, oriented single crystal samples were characterized using orientation imaging microscopy before and after uniaxial tensile deformation. The deformation characteristics are compared with model simulations using crystal plasticity finite element model simulations.

INTRODUCTION

Deformation studies of single crystal niobium and the microstructures produced are useful for several reasons. First, as the SRF community explores the use of large grain (or possibly single crystal) sheets or tubes, practical knowledge of how these will deform using different forming methods (deep drawing, hydroforming) is needed. Second, relating deformation texture through the deformed microstructure to recrystallized texture would allow engineering of desired recrystallization textures. A crystal plasticity finite element model addresses both needs, as simulations of single crystal deformation aid in determining active slip systems and resulting material properties. These enable the more complex simulations of forming that may be used to guide decisions of which crystal orientations or textures to use for a given forming operation.

Plastic deformation occurs by the motion of dislocations, which eventually form dislocation substructures as they interact with each other and other lattice defects. Greater understanding of which slip systems are active for various crystal orientations and the dislocation substructure their interaction produces is needed to predict subsequent recrystallized orientations. For example, the commonly used polycrystalline sheet began as a large-grained ingot in which each grain deformed according to its active slip systems during forging and rolling. This leads to various dislocation substructures, deformation textures, and eventually recrystallization textures present in each ingot grain's former volume, resulting in overall texture variations. even within batches from the same manufacturer.

*Work supported by FNL, DOE (ILC)
#baarsder@msu.edu

MATERIALS & ANALYTICAL METHODS

Single crystal Nb samples were cut from a disc that had been sliced from an ingot obtained from Ningxia. Orientation imaging microscopy was used to find orientation of each of the grains in the slice. Using these orientations, uniaxial tension stress was computationally applied to each grain orientation in every radial direction, so that the Schmid factors (resolved shear stress) on all slip systems could be identified. Tensile specimen orientations were chosen to favor particular slip systems or combinations of slip systems.

Dog-bone shaped tensile coupons were cut from individual grains using electro-discharge machining (EDM). The gage length was 18mm with 1mm fillets at the shoulders, 4mm wide, and 2.8mm thick; each grip section length was 10mm, 6mm wide, and 2.8mm thick. Samples were then polished to mirror finish by alternating between chemical etching (80% Nitric and 20% Hydrofluoric acid for 4 minutes) and mechanical polishing steps. The last mechanical polish was to 0.05µm using colloidal silica, followed by electropolishing with 12V at -30°C for 8 min. Orientation imaging microscopy (OIM) was conducted on a Camscan 44FE SEM using a TSL(Link) system to confirm that the initial orientation at the center of each specimen would indeed resolve the desired shear stress onto the desired slip systems as shown in Table 1.

After OIM, samples were mounted in a tensile testing machine (Instron 4302, Instron's Bluehill software) and deformed to 40% engineering strain in uniaxial tension (similar to strains in the iris of an elliptical cavity). After deformation, five OIM scans were made within a few mm of the center of the gage length.

Local average misorientation (LAM) maps highlighted local gradients in lattice orientation over a scanned area of 112x327µm with a step size of 1µm. These maps are formed by comparing each data point to its immediate neighbors, and the difference in orientation displayed using a 0° (blue) to 5° (red) gradient scale, which highlights low-angle grain boundaries and shear bands (sheet-like arrangements of dislocations).

The LAM data are also represented as histograms, which have been shown to be correlated to geometrically necessary dislocation (GND) density; peaks at higher average misorientations imply higher GND content within the crystal lattice [1]. GNDs are unpaired dislocations, often arranged in low-energy configurations, which account for the orientation gradient. This technique does not detect statistically stored dislocations (SSDs), pairs of dislocations with opposite sign that could recombine into a whole plane if they met. These pairs cancel each other's

contribution to misorientation of the lattice. In a worked metal with no heat treatment, the SSD density is much greater than GND density. [2]

An optimized crystal plasticity finite element modelling (CPFEM) approach was used to predict active slip systems based on each single crystal specimen's initial orientation, assuming that slip on {110} planes had the lowest critical resolved shear stress (CRSS), with {112} plane slip having a 20% higher CRSS, and {123} slip was not activated [3,4]. A fine-meshed dog-bone model of the same dimensions as the physical samples was uniaxially deformed using ABAQUS. The boundary conditions were such that one end was held fixed while the other was displaced a set distance at each time step. For each time step, the orientation, stress, and work hardening parameters of each slip system are updated. Predictions of activated slip systems are based on a combined constraints method, which finds the single yield function. By minimizing the single yield function, the active slip systems are chosen. The FEM model is updated to satisfy its requirements, and then proceeds to the next time step [4]. The simulations were conducted to a final strain of 40%. Activation of different slip systems in different crystals was predicted. Some material parameters had already been determined by trial and error to obtain a close fit to previous studies of experimental stress-strain curves [5].

Table 1: Sample names and favored slip systems

Name	Role
P3	same τ on two {112}, different direction
Q2	same τ on a {110} and a {112}, same direction
S3	3.0% more τ on {110} over a {112}, same direction
T3	9.3% more τ on {110} over a {112}, same direction
U3	similar mid τ on 4 planes, 2 different directions
V3	similar high τ on 4 planes, 2 different directions
W3	2.3% more τ on {112} over a {110}, same direction
X3	8.5% more τ on {112} over a {110}, same direction

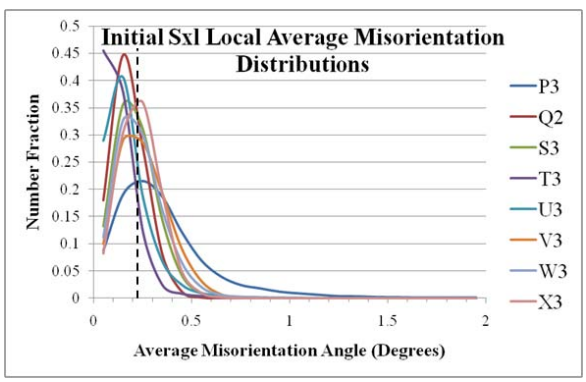

Figure 1: As-polished local average misorientation distributions. Dotted line marks the overall average (0.22°).

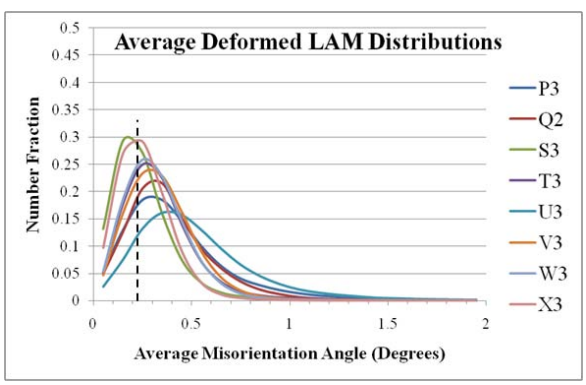

Figure 2: Average of deformed LAM distributions (average of five locations within 3 mm of the center of the gage length of each sample). For comparison, dotted line marks the overall average of the undeformed samples (0.22°)

RESULTS & DISCUSSION

After polishing, the local average misorientation (LAM) histograms show that in general, the various crystal orientations have similar amounts of misorientation (Figure 1), implying similar geometrically necessary dislocation (GND) content. Sample P3 is the most different from the others, and this difference may also be due to incomplete removal of sub-surface damage (in the form of GNDs) introduced during polishing.

After 40% strain, the different orientations show varying amounts of GND content (Figure 2), evident by the decrease in the peak of the histograms and greater spreading to the right. In some orientations, the change was small, implying that dislocations were more able to exit the crystal at free surfaces. The small increase in GND population may be due to active slip systems operating in the same slip direction, but only changing planes, as cross-slip may occur (dislocation motion changes from one plane to another but in the same slip direction). In contrast, orientations with active systems which have different slip directions and planes are more likely to develop dislocation tangles, and retain more GNDs and SSDs. Indeed, Figure 2 shows that samples P3 and U3, each with biased slip systems having different directions, have higher average misorientation angles, and samples S3 and X3 having biased slip systems in the same slip direction have smaller average misorientation angle distributions that are nearly the same as the initial undeformed state. Figures 3 and 4 illustrate these effects using orientation maps of samples P3 and X3 as extreme examples. The LAM map for P3 in Figure 3 shows two directional features related to slip in two directions, while the color gradients show alternating regions of orientation change in direction different from the sharper lines (positive sloped shear bands). In contrast, the maps for X3 in Figure 4 are nearly featureless; only the change in orientation from the initial undeformed state (white prism) shows that deformation occurred. Figure 5 shows changes in orientation in detail along an approximately 300 µm long line across P3 (equally favored slip on two

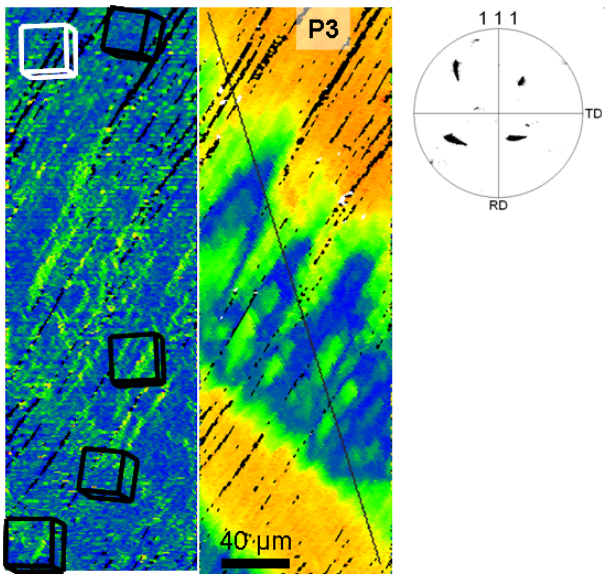

Figure 3: Sample P3. Left to right: LAM map (0 blue to 5° red) showing regions with significant GND dislocation substructure. White prism is initial crystal orientation, black prisms show different orientations within the scan area. Crystal Orientation map of misorientations relative to an orientation in the center of the map (0 blue to 20° red), Pole Figure showing more spread of <111> slip directions due to deformation (<111> direction is vector coming out the prism corners).

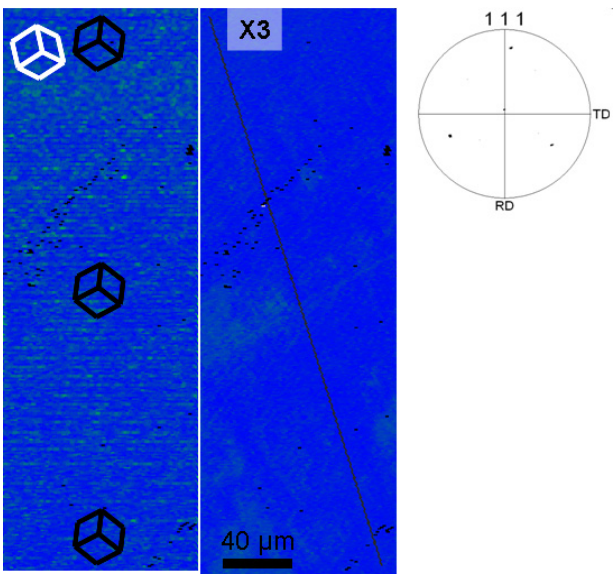

Figure 4: Sample X3, 1µm step. Left to right: LAM map (0 blue to 5° red) showing a lack of GND dislocation substructure. White prism is initial crystal orientation, black prisms show different orientations within the scan area. Crystal Orientation map of misorientations relative to an orientation in the center of the map (0 blue to 20° red), and the pole figure shows almost no spread of <111> slip directions due to deformation (<111> direction is vector coming out the prism corners).

{112} planes in different directions), showing heterogeneous orientations, while X3 (favored for single slip on {112}), shows almost no variations in orientation. These differences are evident also in the (111) pole figures, where the single slip in X3 results in no peak spreading, while the bands of alternating lattice rotation in P3 reflect heterogeneous rotations evident as streaks in different directions in 3 of the 4 poles of the pole figure. The other samples fall between these extremes, and may reflect the fact that in BCC crystals, a high resolved shear does not necessarily mean a slip system will be active, and so the actual actived slip systems may be different from those originally biased [6,7].

The stress-strain curves in Figure 6 also indicate varying degrees of work hardening (increasing amount of stress required to achieve greater strain) that are consistent with the same trends as the LAM data (Figure 3). The plateau regions of Q2, S3, and X3 are longer and indicate more extensive single slip than in the other samples. The change in slope after the plateau indicates activation of at least one additional slip system that causes an increase in dislocation entanglement. In contrast, U3 indicates no single slip as rapid, extensive work hardening occurred, and the specimen reached a condition of unstable flow (ultimate tensile stress) prior to 40% strain.

Initial results From CPFEM analysis shows qualitative agreement between computational modeling and the deformed samples. The slip systems predicted as most active by CPFEM are among those initially biased for high resolved shear. The simulated deformed sample shapes are also in agreement with the deformed samples in that they shear in the same sense (Figure 7). Figure 8 shows three load-displacement curve from the CPFEM model, which shows that single slip on {112} planes is easier than the model predicts. Thus, further work is needed to accurately model the flow characteristics of high purity niobium. The models will need optimization to insure that they can predict activated dislocation systems for arbitrary stress states and crystal orientations.

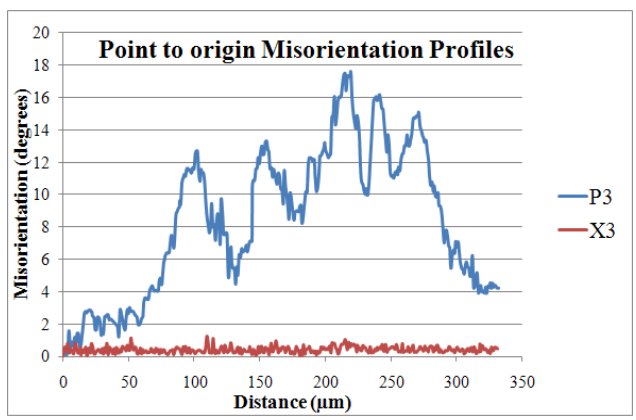

Figure 5: Comparison of point to origin misorientation from upper left to lower right along the black line in Figures 3 and 4. Misorientation in P3 is very heterogeneous compared to X3.

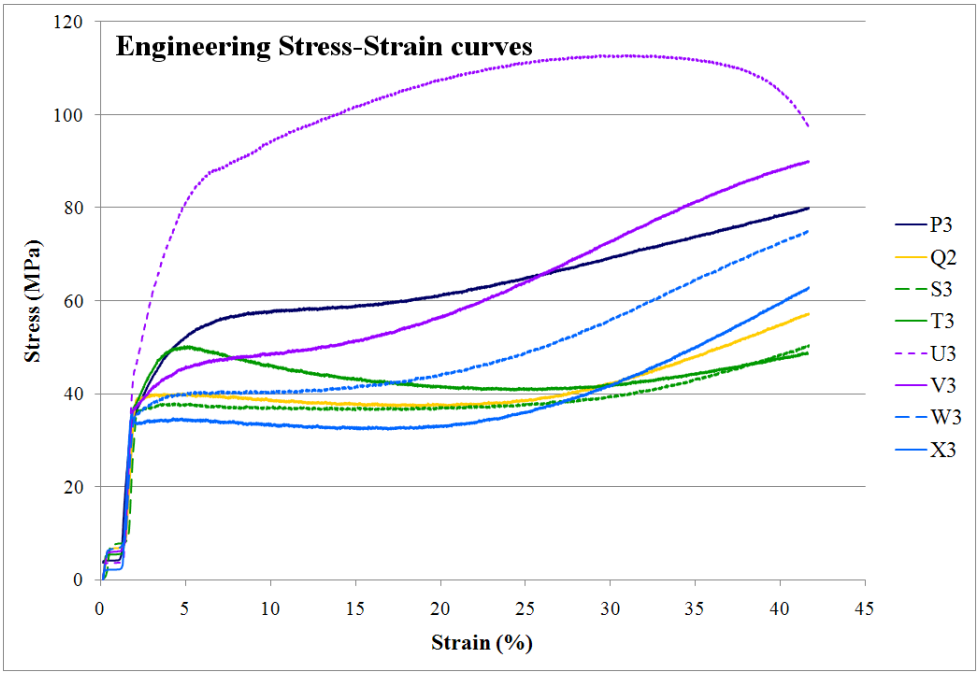

Figure 6: Engineering stress-strain curves for the different single crystal orientation samples.

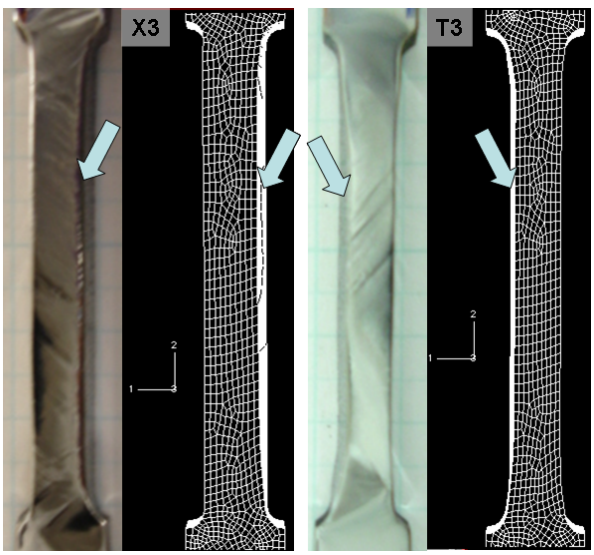

Figure 7: Left: Actual deformed samples X3, T3. Right: CPFEM deformed simulations. Blue arrows indicate the side face that becomes visible as gage length shears, simulations show same sense of shear.

FUTURE WORK

Clear identification of activated slip systems is ongoing, so that an accurate set of rules for slip in high purity Nb can be developed. These specimens will be etched to observe effects of dislocation content on surface roughness, and later cut and welded together in a similar manner as described in [3].

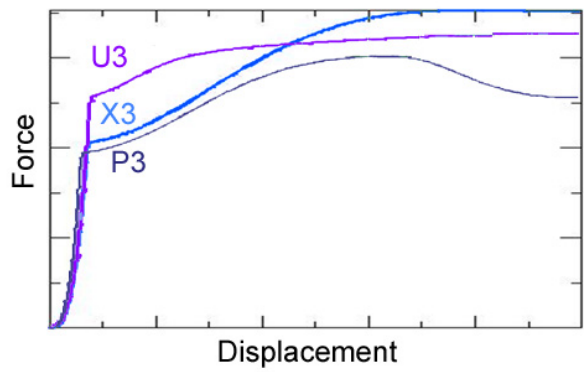

Figure 8: Force-displacement curve for orientations U, X, and P from the CPFEM samples indicate that the assumed relative flow stress rules in the CPFEM model are not yet accurate.

REFERENCES

[1] A. J. Schwartz, M. Kumar, and B. L. Adams, editors, Electron Backscatter Diffraction in Materials Science, Kluwer Academic/Plenum Publishers, 2000.

[2] R.D. Doherty, D.A. Hughes, F.J. Humphreys, J.J. Jonas, D. Juul Jensen, M.E. Kassner, W.E. King, T.R. McNelley, H.J. McQueen, A.D. Rollet, Current issues in recrystallization: a review, Materials Science and Engineering, A238, pp. 219-274, 1997.

[3] D. Baars, T.R. Bieler, A. Zamiri, F. Pourboghrat, C. Compton, SRF 2007 Beijing, China, Oct. 14-19, TUP05, http://web5.pku.edu.cn/srf2007/.

[4] A. Zamiri, F. Pourboghrat,"A novel yield function for single crystals based on combined constraints

optimization," , International Journal of Plasticity, Accepted
[5] D. Baars, H. Jiang, T.R. Bieler, A. Zamiri, F. Pourboghrat, and C. Compton, Ceramic Trans. 201, (2008) 391.
[6] D.K. Bowen, J.W. Christian, G. Taylor. Deformation Properties of Niobium Single Crystals. Can. J. Phys., 45, 903, 1967.
[7] A. Seeger, U. Holzwarth. Slip planes and kink properties of screw dislocations in high-purity niobium. Philosophical Magazine, Vol. 86, Nos. 25-26, 3861-3892, 1-11 September 2006.